Decoration of voids with rhenium and osmium transmutation products in neutron irradiated single crystal tungsten

Matthew J. Lloyd [a,b,*], Robert G. Abernethy [a,b], Mark R. Gilbert [b], Ian Griffiths [a], Paul A.J. Bagot [a], Duc Nguyen-Manh [b], Michael P. Moody [a], David E.J. Armstrong [a]

[a] Department of Materials, University of Oxford, Parks Road, Oxford OX1 3PH, UK
[b] Culham Centre for Fusion Energy, Culham Science Centre, Abingdon, Oxfordshire, OX14 3DB, UK

ABSTRACT

High temperature, neutron irradiated single crystal tungsten, with a post irradiation composition of W - 1.20 $\pm$ 0.11 at.%Re - 0.11 $\pm$ 0.05 at.%Os - 0.03 $\pm$ 0.01 at.%Ta was characterised using a combination of Atom Probe Tomography (APT) and Scanning Transmission Electron Microscopy (STEM). APT showed that within nanoscale clusters of Re/Os, the atomic density was above the theoretical limit. Complimentary High Angle Annular Dark Field (HAADF) imaging shows that some clusters contain voids at their centre which are leading to APT aberrations and enhancing the atomic density. High resolution Energy Dispersive X-ray (EDX) spectroscopy shows that voids are decorated with a shell of rhenium with a small osmium cluster to one side.

© 2019 Published by Elsevier Ltd on behalf of Acta Materialia Inc.

A demonstration fusion power station (DEMO) relies on the development of plasma facing materials that can reliably withstand the combined effects of a large applied heat flux (10–20 MW m^{-2} [1]) and a large dose of 14 MeV neutrons. Tungsten is currently the leading candidate material because it has a high melting temperature (3695 K [2]), a good thermal conductivity and a high resistance to sputtering through interaction with the plasma [3]. Radiation damage and transmutation at high operating temperatures (~1300 K [4]) results in an increase of the inherent brittleness of tungsten, and causes an increase in its already high ductile to brittle transition temperature (DBTT) at (673–773 K [5]). Transmutation occurs through a sequence of neutron reactions and nuclide decays within the wall material. The beta decay of W after neutron absorption produces Re, Os, while Ta is produced via the beta decay of other W isotopes that have undergone neutron loss (n,2n) reactions. As a result, the material composition varies significantly with exposure time [6,7]. Spatial variations in the neutron flux and localised moderation also result in considerable variation in the composition of components within the reactor [7]. Understanding how these transmutation products accumulate is important for efforts to predict changes in physical properties of the plasma facing component during their lifetimes. Currently there is little reported data on tungsten samples with realistic transmutation product contents produced by neutron irradiation at reactor relevant temperatures.

In this study, neutron irradiated single crystalline W was investigated using a combination of Atom Probe Tomography (APT), High Angle Annular Dark Field (HAADF) imaging and Energy Dispersive X ray (EDX) mapping. Pure W samples were irradiated at the High Flux Reactor (HFR) at Petten for a total of 208 full power days at 900 °C, as part of the Extremat II program, resulting in a total dose of 1.67 dpa. For more information on the irradiation, the reader is referred to [8]. APT and TEM samples were prepared using a Focussed Ion Beam (FIB) lift out technique with a FEI Helios FIB-SEM, at the Materials Research Facility (MRF) CCFE [9]. For APT, the lifted out material was mounted onto silicon posts using Pt deposition and sharpened using a series of successively smaller annular milling patterns (beam currents 1.5 nA–40 pA, acceleration voltage of 30 kV) until the tip of the needle was between 50 and 100 nm in diameter. A final polishing stage using an acceleration voltage of 2 kV and a beam current of 300 pA was used to remove approximately 500 nm of material to minimise any Ga implantation. For TEM, thinning was carried out at 30 kV using successively lower beam currents, with a final thinning stage at 2 kV, using a 200 pA beam current at 45° until the lift out was transparent under a 10 kV electron beam. Flash polishing was carried out in a 0.5%NaOH solution with a 10 V, 50 ms applied voltage. The samples were then cleaned in methanol and plasma cleaned for 120 s using a Fischione 1020 plasma cleaner.

APT was carried out in laser mode in a CAMECA LEAP® 5000 XR using a sample temperature of 55 K, a laser pulse energy of 125 pJ and a pulse frequency of 100 kHz. The data was reconstructed and visualised using IVAS® 3.8.2. Fig. 1a shows a portion of the mass spectrum obtained during APT with the peaks ranged as W, Ta, Re and Os
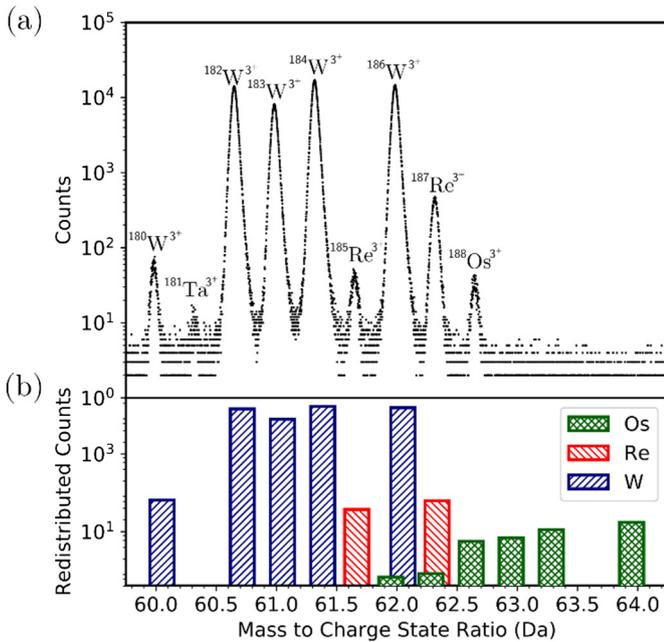
Fig. 1. (a) Sub-section of a representative mass spectrum generated by APT analysis. Labels indicate the isotopic assignment for all reconstructed ions contributing to that peak, respectively. (b) Expected relative size of peaks if isotopes were in natural abundances. Total counts from APT for each element in the mass spectrum shown in (a) have been summed and multiplied by the natural abundance of that element.

highlighted, compared in Fig. 1b with the expected isotopic distribution of these elements, based on the natural abundances. During conventional reconstruction of data, the ratios of the peaks can be expected to follow the natural isotopic distribution, and can therefore be used to identify peak species and prevent erroneous ranging. However, in the samples studied here, the Re, Os and Ta are introduced artificially through transmutation and therefore do not follow the natural abundances. Based on comparison with FISPACT-II [10] modelling (see Table 1), and to EDX measurements carried out elsewhere by Klimenkov et al. [8], the assumption was made that the overlaps between Re, Os and Ta in the 61.67, 62, 62.33 and 62.67 Da peaks were negligible and could be ranged as ^{185}Re, ^{186}W, ^{187}Re and ^{188}Os respectively. The entire Os signal used for this analysis came from the ^{188}Os peak. This resulted in a bulk sample composition of W W - 1.20 ± 0.11 at.%Re - 0.11 ± 0.05 at.%Os - 0.03 ± 0.01 at.%Ta in good agreement with FISPACT modelling and EDX measurements which predicted W-1.4Re-0.10s [8]. The uncertainty on the composition was estimated by comparing the result when peaks in the mass spectrum were ranged background-to-background and at the full width half maximum (FWHM), rather than taking the counting uncertainty which is much lower. The results presented in Table 1 indicate that FISPACT-II is a very reliable approach to simulating the transmutation of these alloys and provides a robust description of post irradiation composition.

Fig. 2 shows one of the APT samples analysed, reconstructed using an initial tip radius estimated by IVAS and using the voltage profile to determine the tip diameter as a function of depth. W atoms are shown in blue, Re in red and Os in green. Ta atoms are not shown as they are present only in very small numbers and were uniformly distributed throughout the specimen. Red and green isoconcentration surfaces are displayed for 5 at.%Re and 1.5 at.%Os respectively. There is clear segregation of Re and Os from the matrix and a substantial increase in the Re and Os concentration compared to the nominal concentration. Furthermore, Os is seen to be located at the centre of the larger Re precipitates.

33 dpa ion implantations at 573 and 773 K have been conducted by Xu et al. in both binary W-2Re [4,11] and ternary W-2Re-1Os [11]. Their APT of these samples showed both the formation of Re rich clusters in the binary alloy and smaller Os rich clusters in the ternary. At 773 K, small Os clusters were found to form preferentially to Re, inhibiting the formation of Re clustering seen in the binary alloy, but with some Re attachment to the Os cluster.

Xu et al.'s work used ion irradiation as a surrogate for neutrons, which is a commonly used technique of introducing point defects into a material. This results in a far higher dose rate than seen in the neutron irradiated specimens studied here. In the case of the neutron irradiated samples, the defects have more time to migrate through the material and drag Os and Re. The results shown in Fig. 2 are consistent with the initial formation of a small Os cluster due to its higher binding energy to vacancies [12], which are known to form voids in neutron irradiated W [13]. Os segregation to grain boundaries and dislocations within tungsten was observed in early atom probe field ion microscopy work in the 1980's by Eaton and Nordén [14]. These Os clusters could act as a nucleation sites for the Re, which forms around the Os over time.

Void formation is known to occur in neutron irradiated W samples [13]. The impact of voids on the reconstruction of APT data is not fully understood, with some studies showing an apparent decrease in density that the authors interpret as the location of a void [15], whilst others indicate an apparent increase in the density due to the effects of a higher atomic evaporation at the periphery of the void and the focussing of the evaporated ion flight path [16,17]. By binning a region of the APT data into voxels using IVAS, a map of the specimen density in number of atoms per cubic nanometre can be produced, as shown in Fig. 3, by counting the number of atoms per voxel. A density map of the sample is shown in Fig. 3a. There is a clear increase in the atomic density associated with the Re/Os clusters, the location of which are shown in Fig. 3b and c. Re has a lower evaporation field threshold and therefore high localised concentrations of Re could contribute to an increase in the observed density, however, this is typically lower than observed here. At the centre of the Re clusters shown in Fig. 3, the measured atomic density from APT is ~80 atoms nm^{-3}. Bulk density measurements from APT are lower than the theoretical atomic density as APT does not detect 100% of the atoms. Despite this, the measured core density of the clusters is above the theoretical maximum atomic density of tungsten (62.84 atoms nm^{-3}) which is bcc and has a lattice parameter of 3.1690 Å. This indicates that the clusters observed may be decorating voids which have the potential to produce this apparent increase in atomic density through trajectory aberration at the periphery of the void.

A combination of STEM HAADF and EDX mapping was carried out using a JEOL 200F ARM TEM, operating at 200 kV and equipped with a
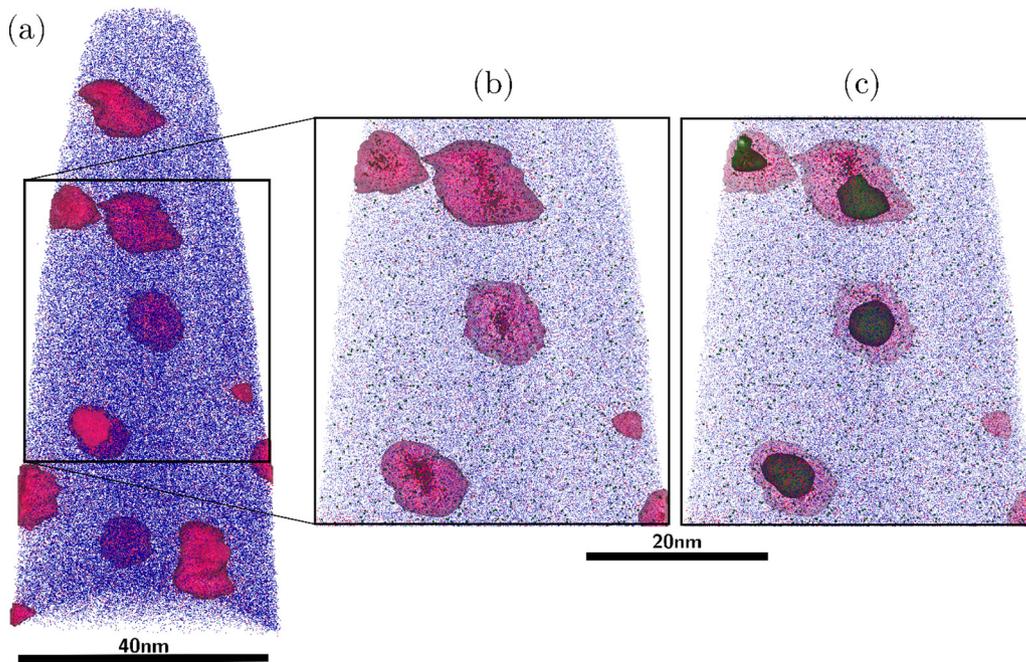
Table 1

Comparison between the calculated distribution of isotopes and the measured distribution from APT produced by transmutation, as a percentage of the total number of atoms in the simulation and the total number of ranged ions in APT. The 11 most commonly occurring isotopes from the simulation are included, isotopes with lower concentration could not be separated from background using APT. Uncertainty on the concentration from APT is estimated by comparing different ranging approaches, background-to-background and at FWHM. A further 60+ isotopes were predicted in lower concentrations. FISPACT-II calculations were performed with appropriate self-shielding and correctly simulated neutron spectra for the EXTREMAT-II experiment and used TENDL-2015 nuclear data as input — see [7] for further details. The simulations even accounted for a change in location of the sample after 60 days of exposure. The results also account for the approximately 6 years of decay cooling between the end of irradiation and APT/EDX measurements.

Nuclide	FISPACT-II %	APT %
^{184}W	30.97	30.98 ± 0.20
^{186}W	26.99	26.78 ± 0.17
^{182}W	25.35	25.39 ± 0.22
^{183}W	15.02	14.84 ± 0.02
^{187}Re	1.34	1.05 ± 0.07
^{188}Os	0.10	0.10 ± 0.03
^{180}W	0.10	0.13 ± 0.02
^{185}Re	0.09	0.12 ± 0.04
^{181}Ta	0.02	0.03 ± 0.01
^{186}Os	0.01	Undetectable
^{189}Os	2.1×10^{-3}	Undetectable

Fig. 2. APT reconstruction of neutron irradiated sample. (a) For visual clarity, only 1.3% of total detected W ions are shown in blue, all detected Re and Os ions are shown in red and green respectively. Red surfaces represent Re isoconcentration surfaces plotted at 5 at.%Re. (b) Higher magnification of the region of interest showing Re isoconcentration surfaces at 5 at.%Re and individual Os atoms as green squares. (c) Region of interest showing transparent Re isoconcentration surfaces and green Os isoconcentration surfaces at 1.5 at.%Os.

JEOL Centurion EDX detector and a Gatan GIF. This was used to map the Re/Os concentration around dark spots in the HAADF image, which suggested the presence of voids. This was confirmed using Electron Energy Loss Spectroscopy (EELS) thickness measurements which showed the darker regions corresponded to a smaller sample thickness. EDX mapping was carried out on a region containing several voids which indicated the presence of Os and Re. The Lα peaks of Re, Os and W at 8.651 eV, 8.910 eV and 8.396 eV were used to identify the atomic
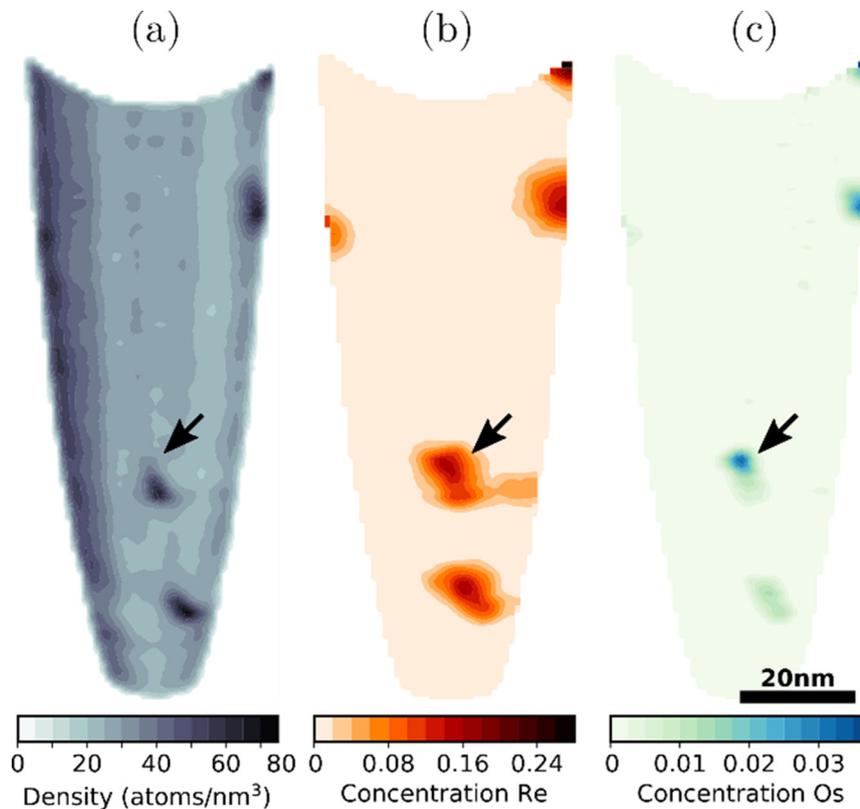

Fig. 3. 5 nm cross section of the atom map shown in Fig. 2. (a) Density contour in number of atoms per cubic nm (b) Re concentration contour (c) Os concentration contour. Arrow indicates central precipitate with Os rich zone offset from higher density region.

species. To reduce drift artefacts, the EDX was performed using multiple scans and a fast acquisition time.

A large population of voids was seen as well as smaller isolated bright spots in the HAADF image which were confirmed to be Re clusters using EDX mapping. Fig. 4a shows a high magnification STEM HAADF image of a single void, confirmed to be a void using EELS line scans. Fig. 4c, d and e show the W, Re and Os EDX maps of this area respectively. The Re appears to form a shell around the void with a precipitate offset to one side. Within this offset region is the Os precipitate. This is further evidenced by the APT data shown in Fig. 3c, where the central precipitate also shows an offset of the osmium rich region compared to the rhenium one.

The samples studied here represent the upper right portion of the structural diagram for the irradiated W microstructure as a function of dose and temperature produced by Hasegawa et al., which also have a microstructure dominated by voids [13]. Several neutron irradiation studies using fission neutron spectra have shown the formation of lenticular chi or sigma phase precipitates [18–21], however the post

Fig. 4. (a) Lower magnification and (b) high magnification High Angle Annular Dark Field (HAADF) images of voids in neutron irradiated single crystal W. EDX maps of (c) W, (d) Re and (e) Os showing the decoration of central void.

irradiation compositions of these samples is typically much higher than can be expected for fusion wall materials. Klimenkov et al. found Re/Os precipitates in the same material as studied here but only a small Os signal was observable. Re was shown to segregate to the grain boundaries in these samples but Os was not shown in this region [8]. By using APT here we are able to separate and map both Re and Os. Hwang et al. saw both Re and Os within small clusters in neutron irradiated (initially pure) W, transmuted to 4%Re-0.8%Os using APT. Os was present within the clusters but was not seen to form a core region of Os as seen here. The regular separation of the clusters indicated that they had formed on a void lattice, however there was no direct indication from atomic density mapping if voids had affected the internal structure of the clusters [19].

The mechanism through which this precipitation occurs is not clear. The microstructure presented here is dominated by voids unlike in Xu et al.'s work [4,11] in which there was no indication of voids associated with the Re clusters. This could be due to the lower irradiation temperature and higher dose rate used in Xu et al.'s ion implantation, which may have suppressed void growth, making them more difficult to detect using APT. Kinetic Monte Carlo (KMC) simulations of W—Re have shown the importance of the mixed interstitial for precipitation. Unlike the self-interstitial, which is confined to 1D motion, a mixed W—Re interstitial is able to move through a series of rotations and translations, to effectively migrate in 3D [12,22]. The increased mobility of the mixed interstitial facilitates the nucleation and growth of Re clusters, despite the predicted solid solution [22]. Models such as this rely on a simple Ising like model, which uses pairwise interactions to construct process rates, such as migration and rotation. The pairwise binding energy of the di-vacancy in W is close to zero, which results in an underestimation of the role of vacancies within this model. The use of a Cluster Expansion (CE) Hamiltonian can overcome this problem by considering interactions between 3 or more atoms/defects at once. At high temperatures (stage IV recovery [3]) vacancies become much more mobile and play a more significant role in microstructural evolution. MC simulations using a CE Hamiltonian have predicted the precipitation of Re in W alloys through the formation of small voids, decorated with Re atoms [23], however, the role that Os plays in this process is still being fully investigated. More modelling work is required to understand the operative mechanisms during irradiation, particularly when in the presence of Os.

In summary, neutron irradiation of pure single crystal W led to the formation of a W-1.20 $\pm$ 0.11 at.%Re-0.11 $\pm$ 0.05 at.%Os-0.03 $\pm$ 0.01 at.%Ta alloy. Comparison between FISPACT-II results and APT demonstrated that FISPACT-II is a very reliable way of quantifying transmutation in neutron irradiated material. This sample is of particular importance for the study of the evolution of materials in a fusion environment as it has undergone a high temperature irradiation and has a transmutation induced composition similar to a W first wall component after several years of operation in a reactor. Under irradiation APT showed clusters of mainly of Re, with Os at the centre, which were on average 8 nm in diameter. Analysis of the reconstruction indicated that voids within the clusters may have contributed to an artefact which could have disrupted the inner structure of the clusters seen in APT. Additionally, STEM HAADF and EDX of the sample confirmed that clustering can occur through the decoration of a void and likely contributed to the structure seen in the APT analysis. This work shows the importance of using transmutation compositions when ranging the APT data produced on samples containing non-natural abundances of elements, and raises questions about the validity of using ion implantation which typically does not facilitate void formation. New neutron irradiation campaigns, and more modelling studies, which include the full range of transmutation products are needed to fully understand the impact transmutation will have in a reactor. In addition, care must be taken if only using APT to study precipitation in tungsten and other alloys that can undergo void formation during irradiation, as artefacts can be induced into data reconstruction due to trajectory aberrations around
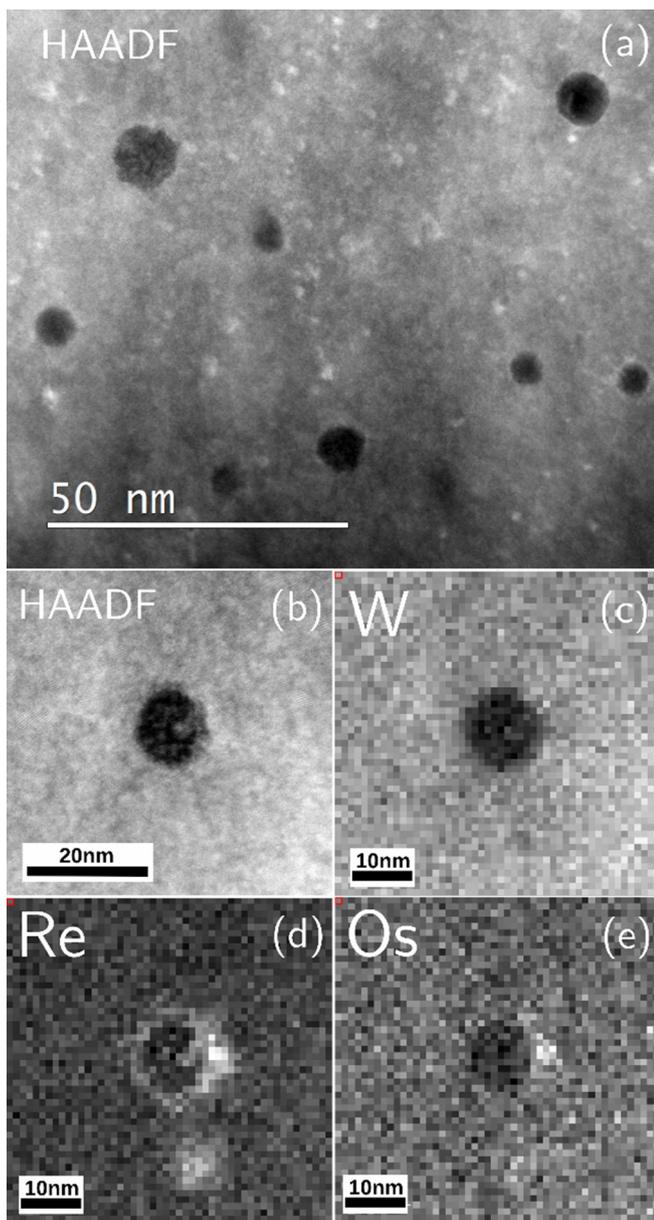
the void. Further work is need on methods used to reconstruct the APT data to include the voids seen in HAADAF and account for localised magnification. The data obtained in this study is available from [24].

Acknowledgements

References

[1] J. Matejicek, M. Battabyal, P. López-Ruiz, M. Celino, J. Linke, J.G. van der Laan, C.S. Becquart, H. Li, S. Wahlberg, W.W. Basuki, K. Heinola, J. Riesch, C. Linsmeier, T. Weitkamp, J. Aktaa, L. Romaner, M. Rosiński, S. Lindig, J. Brinkmann, J. Opschoor, S. Giusepponi, A. Hoffmann, W. Schulmeyer, R. Pippan, H. Boldyryeva, L. Veleva, D. Nguyen-Manh, F. Koch, T. Palacios, T. Ahlgren, D.E.J. Armstrong, L. Ciupinski, M.A. Yar, H. Traxler, J. Reiser, A. Muñoz, C. Domain, C. García-Rosales, M.R. Gilbert, A. Ureña, M. Sanchez, S.L. Dudarev, M. Balden, M. Rieth, M. Muhammed, M. Muzyk, N. Holstein, T. Weber, D. Blagoeva, J.H. You, H. Maier, A. De Backer, N. Baluc, J. Gibson, G. Pintsuk, M.-F. Barthe, S.M. Gonzalez de Vicente, J.B. Correia, S. Wurster, K. Nordlund, B. Gludovatz, M. Walter, H. Greuner, W. Krauss, N. Ordás, S.G. Roberts, E. Gaganidze, T. Höschen, T.P. Mishra, S. Antusch, A. Zivelonghi, J. Nucl. Mater. 432 (2012) 482–500.
[2] D.E.J. Armstrong, P.D. Edmondson, S.G. Roberts, Appl. Phys. Lett. 102 (2013), 251901.
[3] R.G. Abernethy, Mater. Sci. Technol. 0836 (2016) 1–12.
[4] A. Xu, D.E.J. Armstrong, C. Beck, M.P. Moody, G.D.W. Smith, P.A.J. Bagot, S.G. Roberts, Acta Mater. 124 (2017) 71–78.
[5] F. Ferroni, X. Yi, K. Arakawa, S.P. Fitzgerald, P.D. Edmondson, S.G. Roberts, Acta Mater. 90 (2015) 380–393.
[6] M.R. Gilbert, J.-C. Sublet, Nucl. Fusion 51 (2011), 043005.
[7] M.R. Gilbert, J.C. Sublet, S.L. Dudarev, Nucl. Fusion 57 (2017), 044002.
[8] M. Klimenkov, U. Jäntsch, H.C. Schneider, D.E.J. Armstrong, J. Gibson, Nucl. Mater. Energy 9 (2016) 480–483.
[9] Materials Research Facility, Developing Materials for the Nuclear Industry, 2018.
[10] J.C. Sublet, J.W. Eastwood, J.G. Morgan, M.R. Gilbert, M. Fleming, W. Arter, Nucl. Data Sheets 139 (2017) 77–137.
[11] A. Xu, C. Beck, D.E.J. Armstrong, K. Rajan, G.D.W. Smith, P.A.J. Bagot, S.G. Roberts, Acta Mater. 87 (2015) 121–127.
[12] T. Suzudo, M. Yamaguchi, A. Hasegawa, Model. Simul. Mater. Sci. Eng. 22 (2014).
[13] A. Hasegawa, M. Fukuda, S. Nogami, K. Yabuuchi, Fusion Eng. Des. 89 (2014) 1568–1572.
[14] H.C. Eaton, H. Nordén, Scr. Metall. 17 (1983) 1043–1046.
[15] M.K. Miller, L. Longstreth-Spoor, K.F. Kelton, Ultramicroscopy 111 (2011) 469–472.
[16] P.J. Birdseye, D.A. Smith, G.D.W. Smith, J. Phys. D. Appl. Phys. 7 (1974) 1642–1651.
[17] M. Dagan, L.R. Hanna, A. Xu, S.G. Roberts, G.D.W. Smith, B. Gault, P.D. Edmondson, P.A.J. Bagot, M.P. Moody, Ultramicroscopy 159 (2015) 387–394.
[18] X. Hu, T. Koyanagi, M. Fukuda, Y. Katoh, L.L. Snead, B.D. Wirth, J. Nucl. Mater. 470 (2016) 278–289.
[19] T. Hwang, A. Hasegawa, K. Tomura, N. Ebisawa, T. Toyama, Y. Nagai, M. Fukuda, T. Miyazawa, T. Tanaka, S. Nogami, J. Nucl. Mater. 507 (2018) 78–86.
[20] X. Hu, C.M. Parish, K. Wang, T. Koyanagi, B.P. Eftink, Y. Katoh, Acta Mater. 165 (2019) 51–61.
[21] X. Hu, N.A.P.K. Kumar, T. Koyanagi, Y. Katoh, L.L. Snead, T. Hwang, L.M. Garrison, J. Nucl. Mater. 490 (2017) 66–74.
[22] C.H. Huang, L. Gharaee, Y. Zhao, P. Erhart, J. Marian, Phys. Rev. B 96 (2017) 1–17.
[23] J.S. Wróbel, D. Nguyen-Manh, K.J. Kurzydłowski, S.L. Dudarev, J. Phys. Condens. Matter 29 (2017) 1–5.
[24] M.P.Moody Lloyd, D.E.J. Armstrong, Decoration of Voids with Rhenium and Osmium Transmutation Products in Neutron Irradiated Single Crystal Tungsten, Oxford University Research Archive, 2019 https://doi.org/10.5287/bodleian:PmyPo1aK2.